4.3 OBSERVATIONS OF STORM SCALE BOUNDARY EVOLUTION WITHIN THE 23 MAY 2007 PERRYTON, TX SUPERCELL

Patrick S. Skinner* and Christopher C. Weiss
Texas Tech University, Lubbock, Texas

1. INTRODUCTION

Several studies over the past decade have established a link between tornadic supercells and relatively low thermodynamic deficits in both the Rear-Flank Downdraft (RFD) (Markowski et al. 2002; Grzych et al. 2007) and the Forward-Flank Downdraft (FFD) (Shabbott and Markowski 2006). However, considerable heterogeneity has been observed within individual RFD's (Finley and Lee 2004; Hirth et al. 2008) and the presence of a distinct kinematic and thermodynamic boundary within the forward flank has not always conformed to the examples of observational schematics (Lemon and Doswell 1979) and numerical simulations (Wicker and Wilhelmson 1995).

In order to provide a higher spatial resolution of in-situ observations in hazardous, but potentially critical regions within supercell thunderstorms, Texas Tech University has developed a suite of durable, rapidly deployable surface sensors dubbed StickNet (Weiss and Schroeder 2008). The first mass deployments of these instruments occurred during the Multiple Observations of Boundaries In the Local-storm Environment (MOBILE) project undertaken to sample the forward-flank region of supercells in the late spring of 2007. Twenty-two StickNet probes were available for deployment which, coupled with a four vehicle mobile mesonet, allowed supercells to be sampled at an unprecedented spatial resolution.

This study will focus on observations obtained as a weakly tornadic, high-precipitation supercell in the northeastern Texas Panhandle on May 23rd, 2007 transitioned into a non-tornadic phase. Several features in the analysis will be discussed, including the sampling of an apparent secondary RFD surge with sharp thermodynamic gradients within a broader scale RFD, weak gradients along the forward-flank reflectivity gradient, and possible interaction with a boundary established in prior convection.

Corresponding author address: Patrick S. Skinner, Texas Tech University, Atmospheric Science Group, Department of Geosciences, Lubbock, TX, 79409; e-mail: Patrick.Skinner@ttu.edu

2. DATA COLLECTION AND QUALITY ASSURANCE

2.1 StickNet

Of the twenty-two total StickNet probes, twenty were deployed on May 23rd. Eleven type "A" probes employed a R.M. Young anemometer with nine of these eleven also capable of measuring temperature, humidity and barometric pressure. Though these probes are capable of taking 5 or 10 Hz data, only 1 Hz data are considered in this study. Nine type "B" probes were equipped with a Vaisala all-in-one type instrument that was capable of taking 1 Hz measurements of rain and hailfall as well as temperature, humidity, barometric pressure, wind speed and direction. The position of each probe is determined using an onboard GPS receiver/antenna and the wind direction is corrected for probe orientation using a flux compass.

Four vehicles were responsible for deploying the StickNet array, two pick-up trucks equipped with custom racks capable of carrying five probes and two trucks towing trailers capable of carrying twelve StickNet probes. As only one viable road option was available on May 23rd, a "one road" deployment was initiated approximately seventy-five minutes ahead of the arrival of the target storm's updraft. The two trailers deployed probes at two kilometer intervals centered about a point given by the Field Coordinator (FC) which represents the forecasted center of mesocyclone circulation as the storm crosses the instrument array. The difficulty in maneuvering the trailers requires that they deploy moving from north to south in this experimental design, negating the need to make a u-turn and allowing them to safely exit the storm environment to the south as the primary updraft approaches. The more maneuverable trucks without trailers are responsible for deploying a fine-scale array with approximately one kilometer spacing about a continuously updated forecasted mesocyclone position. As these vehicles were better able to make u-turns and had less exposure to straight-line winds, they remained in the storm environment longer to more accurately deploy the final probes. All vehicles complete deployments at least fifteen minutes before the center of circulation crosses the array.

Instrument biases were determined through two mass tests of the probes, conducted at the start and end of the MOBILE campaign. Additional data issues that were corrected for the May 23rd deployment are as follows:

- Three probes exhibited large wind direction biases (>30°) caused by a dislodging and erroneous reading of the flux compass. These biases were consistent for all deployments after May 23rd and were similarly evident in the end-of-season mass test. Therefore, the wind measurements have been retained in the analysis with the bias correction applied.
- Two probes did not record a compass heading during the deployment. Because both of these probes were in the fine-scale array within the inflow, their wind directions have been estimated by introducing a correction factor based on the average wind direction of the probes in the immediate vicinity.
- Three probes recorded erroneous humidity values. The thermodynamic data from these probes have been neglected for this case.

2.2. Mobile Mesonet

The mobile mesonet used in Project MOBILE comprised of four instrumented vehicles modeled after those in Straka et al. (1996). When collecting data for the May 23rd case, three of these probes conducted roughly three kilometer long transects across the forward-flank reflectivity gradient of the target storm at a constant speed of 50 km/hr. The fourth vehicle was operated by the FC and remained in the inflow region of the storm, allowing the FC to relay transect endpoints to the other vehicles or terminate transects based on the visual and radar characteristics of the storm.

Instrument biases were calculated using an average of one hour of data while the fleet was travelling as a caravan in quiescent conditions prior to convective initiation. Biases were removed according to the standards set by Markowski et al. (2002) and no significant instrument malfunctions occurred during the May 23rd case. In order to remove errors associated with GPS drift, vehicle headings were locked once the velocity fell below 2.57 m s^{-1} (Hirth et al. 2008). Kinematic values were removed for records where changes in the vehicle acceleration vector magnitude were greater than 1 m s^{-2} (Markowski et al. 2002).

3. METHODOLOGY

Virtual potential temperature (θ_v) was calculated without including the effects of liquid water, which will introduce a warm bias for probes deployed in heavy precipitation. It is estimated that probes in greater than 60 dBZ reflectivity will experience positive biases in excess of 2.61 K (Hirth et al. 2008). Equivalent potential temperature (θ_e) was calculated according to Bolton (1980).

Perturbation values of θ_v and θ_e were calculated using subjectively determined inflow values as a base state. Probe 107A was located in close proximity to the storm without experiencing precipitation and was identified as most representative of the inflow conditions. The base state used is a ten minute average of this probe's data as the center of circulation passed through the instrument array (22:45 – 22:55 UTC).

Time-to-space conversion was performed over the same ten minute period used to determine the base state. Due to deviant mesocyclone propagation over the period of interest compared to the remainder of the storm, the storm motion was subjectively calculated using the apex of the RFD boundary observed in imagery from the Shared Mobile Atmospheric Research and Teaching Radar (SMART-R). This method allowed the time-to-space converted observations to remain correctly positioned with respect to the mean position of the supercell, which was assumed to be steady-state through the period.

The time-to-space converted data were then gridded to a two-dimensional domain using a Barnes analysis scheme. A circular radius of influence of roughly twice the average spacing between probes with a smoothing parameter similar to Koch et al. (1983) was used in the analysis.

4. OBSERVATIONS

On May 23rd Project MOBILE targeted convection initiating along a stationary front in the northeastern Texas Panhandle. The initial convection, hereafter “storm A”, rapidly became supercellular. Due to a limited road network, initial deployments began well ahead of storm A along US 83 in the Canadian River Valley south of Perryton. Additional convection, “storm B,” initiated along the target storm’s right rear-flank early into the deployment. Storm B quickly became the dominant cell and operations were suspended on storm A after five probes were deployed. These five probes sampled the outflow boundary of the weakening storm A as it passed through the array. Beginning at 21:28 UTC, a shift from southeasterly to weak, northwesterly winds occurred and was accompanied by a significant drop in both equivalent potential temperature (>8K) and virtual potential temperature (>5K) across the northwestern-most probe (14B). This boundary sagged southeastward across the remainder of the probes over the following thirty minutes as the storm approached (Fig. 1). After 22:16 UTC, the boundary began to retreat northward but it would persist across some portion of the array through the deployment.

Convection continued to develop along the right-rear flank of Storm B and by the time it approached the instrument array it was a high-precipitation supercell embedded in a broken line of thunderstorms stretching northeastward into Oklahoma. Storm B did produce two weak (EF-0), brief (<2 minute) tornadoes at 22:25 UTC and 22:39 UTC, the latter of which dissipated less than five kilometers to the southwest of the nearest StickNet probes (Fig 3A). The precipitation core of storm B began to affect the northwestern portions of the instrument array beginning at 22:30 UTC and the storm was transitioning to a linear, outflow dominant phase as it left the array around 23:00 UTC. The storm did produce two more weak, brief tornadoes to the northeast as it was embedded in an MCS at 23:14 and 23:40 UTC.

Time series of wind speed, direction, equivalent potential temperature, and virtual potential temperature for probes 107A, 214B, 216B, 217A, and 219A between 22:30 and 23:00 UTC were constructed (Fig. 2). Aside from inflow probe 107A, these probes provide the best samples of the storm as it passed through the array. Probe 214B sampled the northern edge of the storm, while probes 216B and 219A sampled the precipitation core and forward flank. Probe 217A sampled the forward-flank reflectivity gradient and the RFD.

Prior to passage of the RFD between 22:45 and 22:50 UTC, probe 217A was located in an area of light precipitation along the forward-flank reflectivity gradient. It can be seen that the probe experienced similar wind speeds and direction to the inflow values during this time. However, there is a small (1-2 K) increase in equivalent potential temperature and a similar decrease in virtual potential temperature from the inflow values. Similar fluctuations were noted with the other probes deployed across the forward-flank reflectivity gradient (Fig. 3). The increase in equivalent potential temperature corresponds to a small increase in dewpoint in this region and the decrease in virtual potential temperature is attributed to a small decrease in temperature. It appears that inflow air is being modified by evaporational cooling as it enters the light precipitation in the forward flank. This trend acts to create both a weak buoyancy and moisture gradient within the inflow of air being drawn into the updraft.

As the rear-flank gust front (RFGF) boundary passed over probe 217A, the wind shifted from an east-southeasterly direction to a more southerly to south-southwesterly direction (Fig. 2). Changes in thermodynamic variables lagged the wind shift by 1-2 minutes but both θ_e and θ_v began decreasing around 22:47 UTC and continued decreasing on average through 22:55 UTC. Though both equivalent and virtual potential temperature decreased within the RFD, θ_e fluctuated throughout the RFD passage while θ_v decreased steadily. Using mobile mesonet observations, Hirth et al. (2008) noted similar behavior within the RFD of a tornadic storm. Unlike the storm studied by Hirth et al. (2008), this storm exhibited very large deficits of both θ_e (>10 K) and θ_v (>5K) in the RFD during this non-tornadic cycle, which agrees with the findings of Markowski et al. (2002) for nontornadic storms.

At 22:30 UTC, probes 216B and 214B were on the cool side of the boundary left by storm A with northwesterly winds and thermodynamic variables cooler than those at 219A (Fig. 2). This boundary passed back northward through the position of 216B beginning at 22:36 UTC. As it passed the winds veered to east-southeasterly and the thermodynamic variables rose slightly to become similar to probe 219A to the south. From this point through 22:49 UTC both 216B and 219A measured a steady decrease in θ_e and θ_v as the precipitation core of storm B passed with maximum $\theta_e(\theta_v)$ deficits of 7K(5K) observed. Beginning at 22:49, probes 216B and

219A experienced a rapid increase in wind speed coupled with a sharp decrease in both θ_e and θ_v, coinciding with the development of a strong mesocyclone signature to the southeast of the probes in SMART-R radial velocity data (Fig. 4). As the storm transitioned from a weakly tornadic phase to a nontornadic phase very cold air was drawn to the surface to the northwest of the center of circulation. Though no measurements are available to the immediate northeast of the weak tornado at 22:39 UTC, the deficits of $\theta_e(\theta_v)$ measured at the period of maximum rotation near 22:50 UTC are 7K(2K) lower than those measured at prior times within the forward flank of the storm.

When applying a time-to-space conversion for these StickNet observations, a striking decline in both equivalent potential temperature and virtual potential temperature (Fig. 5) is clearly coincident with the approach of the developing mesocyclone. Also apparent is a divergent wind pattern between probes 216B and 219A and the convergence and thermodynamic shift associated with the boundary produced by storm A between probes 216B and 214B. The very large deficits to the northwest of the mesocyclone persist through the analysis period as the mesocyclone passes in between probes 219A and 217A. As the center of circulation approaches the array, there appears to be a secondary boundary passage within the RFD, with a divergence signature apparent between the southwesterly winds on the leading edge of the RFGF and southeasterly winds at the two westernmost probes (including 217A) to the south of the circulation center (Fig. 4). During the passage of the secondary boundary at 22:54 UTC, probe 217A experienced a sharp decrease in θ_e of approximately 5 K with a much smaller decrease in θ_v. The presence of a secondary kinematic and thermodynamic boundary within the RFD, in close proximity to the center of circulation, shows multiple forcing mechanisms may be acting simultaneously. Multiple thermodynamic gradients were observed in close proximity to tornadoes by Markowski et al. (2002) and Hirth et al. (2008). However, both storms displaying the secondary gradients were producing strong to violent tornadoes and there was a positive thermodynamic perturbation in the immediate vicinity of the tornadoes. The strongly negative perturbations near the center of circulation in this nontornadic storm support the findings of Markowski et al. (2002) and others. In addition, it appears that the relevant thermodynamic characteristics of air being ingested into the center of circulation may only exist in a narrow annulus around the center for this case.

5. CONCLUSIONS

The 2007 campaign of Project MOBILE utilized twenty-four probes to sample a high precipitation, weakly tornadic supercell with very high spatial resolution. These observations revealed multiple boundaries within the storm, both pre-existing and storm-generated:

- An outflow boundary generated by prior convection within the FFD which was observed to move northward over time with respect to the storm,
- Slightly cooler and more moist conditions with no discernible wind shift across the forward-flank reflectivity gradient,
- A decreasing, but highly variable trend in equivalent potential temperature within the RFD,
- Secondary kinematic and thermodynamic boundaries located in the immediate vicinity of the center of circulation, with markedly cooler thermodynamics than those in the broader FFD and RFD.

The small thermodynamic and kinematic gradients along the forward flank run counter to observational schematics and numerical modeling studies which predict a sharp boundary across the reflectivity gradient, but support recent observational and radar studies (Dowell and Bluestein 2002; Shabbott and Markowski 2006). Additionally, heterogeneity within the RFD and the presence of a secondary boundary adjacent to the low-level mesocyclone shows that air entering the low-level circulation may have a different origin or be heavily modified from parcels within the broader-scale RFD.

6. ACKNOWLEDGEMENTS

The authors wish to thank Ms. Therese Thompson as well as Drs. Lou Wicker, Michael Coniglio, and Michael Biggerstaff for generously providing SMART-R data for the case. Thanks are also extended to Brian Hirth for assistance with the objective analysis software and Jaret Rogers for his help designing the experimental plan. The Unidata-developed Integrated Data Viewer (IDV) and Oklahoma Climatological Survey's WxScope software were used to generate some images within this study. Finally, we are indebted to the volunteers from Texas Tech University and the University of Michigan for their efforts during Project MOBILE.

7. REFERENCES

Biggerstaff, M.I., L.J. Wicker, J. Guynes, C. Ziegler, J.M. Straka, E.N. Rasmussen, A.L. Doggett, L.D. Carey, J.L. Schroeder, and C. Weiss, 2005: The Shared Mobile Atmospheric Research and Teaching (SMART) Radar: A Collaboration to Enhance Research and Teaching. *Bull. Amer. Meteor. Soc.*, **86**, 1263-1274.

Bolton, D., 1980: The computation of equivalent potential temperature. *Mon. Wea. Rev.*, **108**, 1046-1053.

Dowell, D.C., and H.B. Bluestein, 2002: The 8 June 1995 McLean, Texas, storm. Part II: Cyclic tornado formation, maintenance, and dissipation. *Mon. Wea. Rev.*, **130**, 2649-2670.

Finley, C.A. and B.D. Lee, 2004: High resolution mobile mesonet observations of RFD surges in the June 9 Basset, Nebraska supercell during Project ANSWERS 2003. *Preprints, 22nd Conf. on Severe Local Storms*, Hyannis, MA, *Amer. Meteor. Soc.*, P11.3.

Grzych, M.L., B.D. Lee, and C.A. Finley, 2007: Thermodynamic analysis of supercell rear-flank downdrafts from project ANSWERS. *Mon. Wea. Rev.*, **135**, 240-246.

Hirth, B.D., J.L. Schroeder, and C.C. Weiss, 2008: Surface analysis of rear-flank downdraft outflow in two tornadic supercells. *Mon. Wea. Rev.*, **136**, 2344-2363.

Koch, S.E., M. desJardins, and P.J. Kocin, 1983: An interactive Barnes objective map analysis scheme for use with satellite and conventional data. *J. Climate Appl. Meteor.*, **22**, 1487-1503.

Lemon, L.R., and C.A. Doswell III, 1979: Severe thunderstorm evolution and mesocyclone structure as related to tornadogenesis. *Mon. Wea. Rev.*, **107**, 1184-1197.

Markowski, P.M., J.M. Straka, and E.N. Rasmussen, 2002. Direct surface thermodynamic observations within the rear-flank downdrafts of nontornadic and tornadic supercells. *Mon. Wea. Rev.*, **130**, 1692-1721.

Shabbott, C.J., and P.M. Markowski, 2006: Surface in situ observations within the outflow of forward-flank downdrafts of supercell thunderstorms. *Mon. Wea. Rev.*, **134**, 1422-1441.

Straka, J.M., E.N. Rasmussen, and S.E. Fredrickson, 1996: A mobile mesonet for finescale meteorological observations. *J. Atmos. Oceanic Technol.*, **12**, 921-936.

Weiss, C.C. and J.L. Schroeder, 2008: StickNet - A new portable, rapidly-deployable, surface observation system. *Preprints, 24th Conf. on IIPS*, New Orleans, LA, *Amer. Meteor. Soc.*, P4A.1. [Available online at http://ams.confex.com/ams/pdfpapers/134047.pdf.]

Wicker, L.J., and R.B. Wilhelmson, 1995: Simulation and analysis of tornado development and decay within a three-dimensional supercell thunderstorm. *J. Atmos. Sci.*, **52**, 2675-2703.

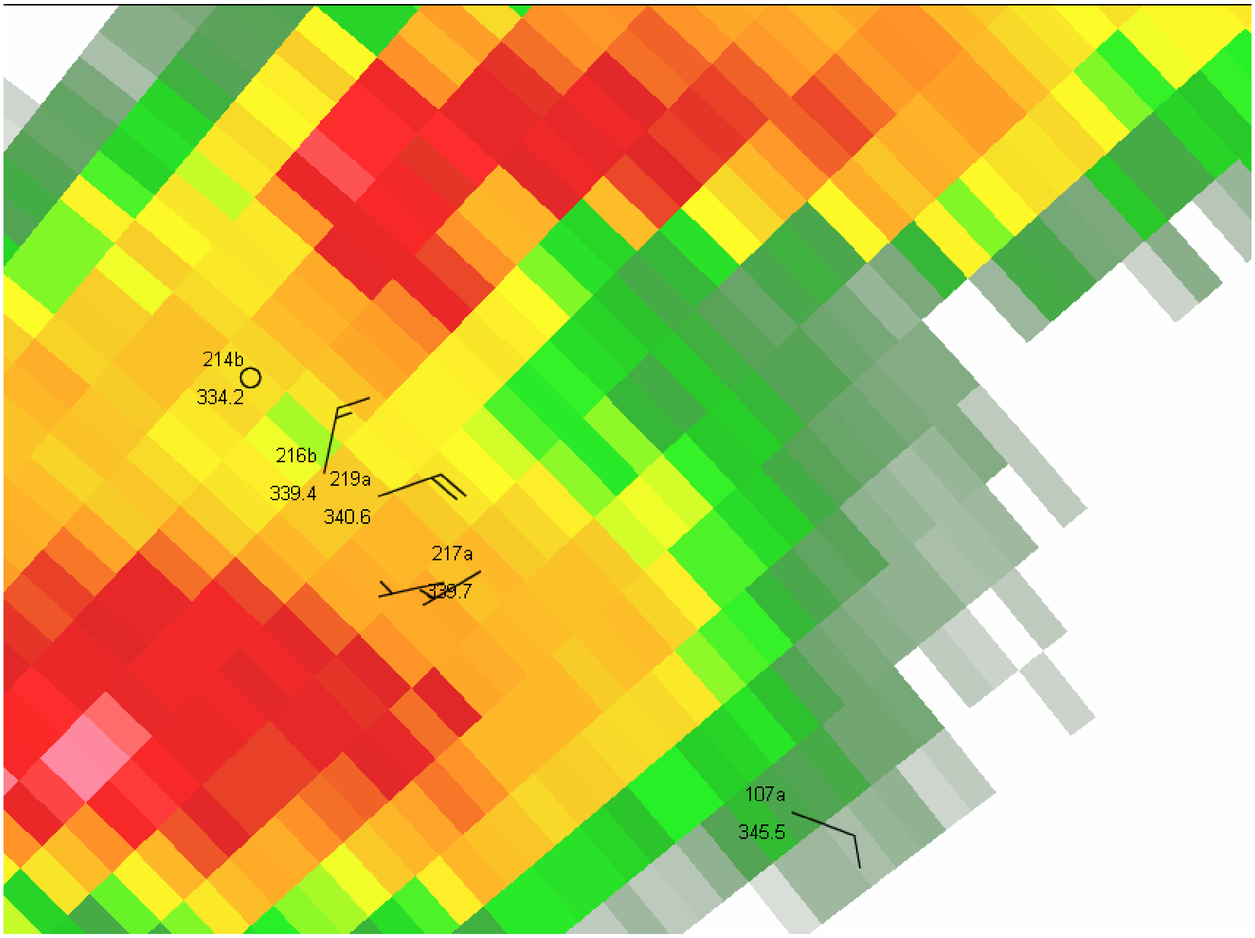

Figure 1: Overlay of StickNet data on KAMA Level II reflectivity data at 22:01 UTC. Wind speed is given in kts, Probe ID appears to the upper-left in the station plot, and equivalent potential temperature (K) in the lower-left. Wind observation to the west-southwest of Probe 217a represents the position of Probe 221A, which only measured kinematics for this case.

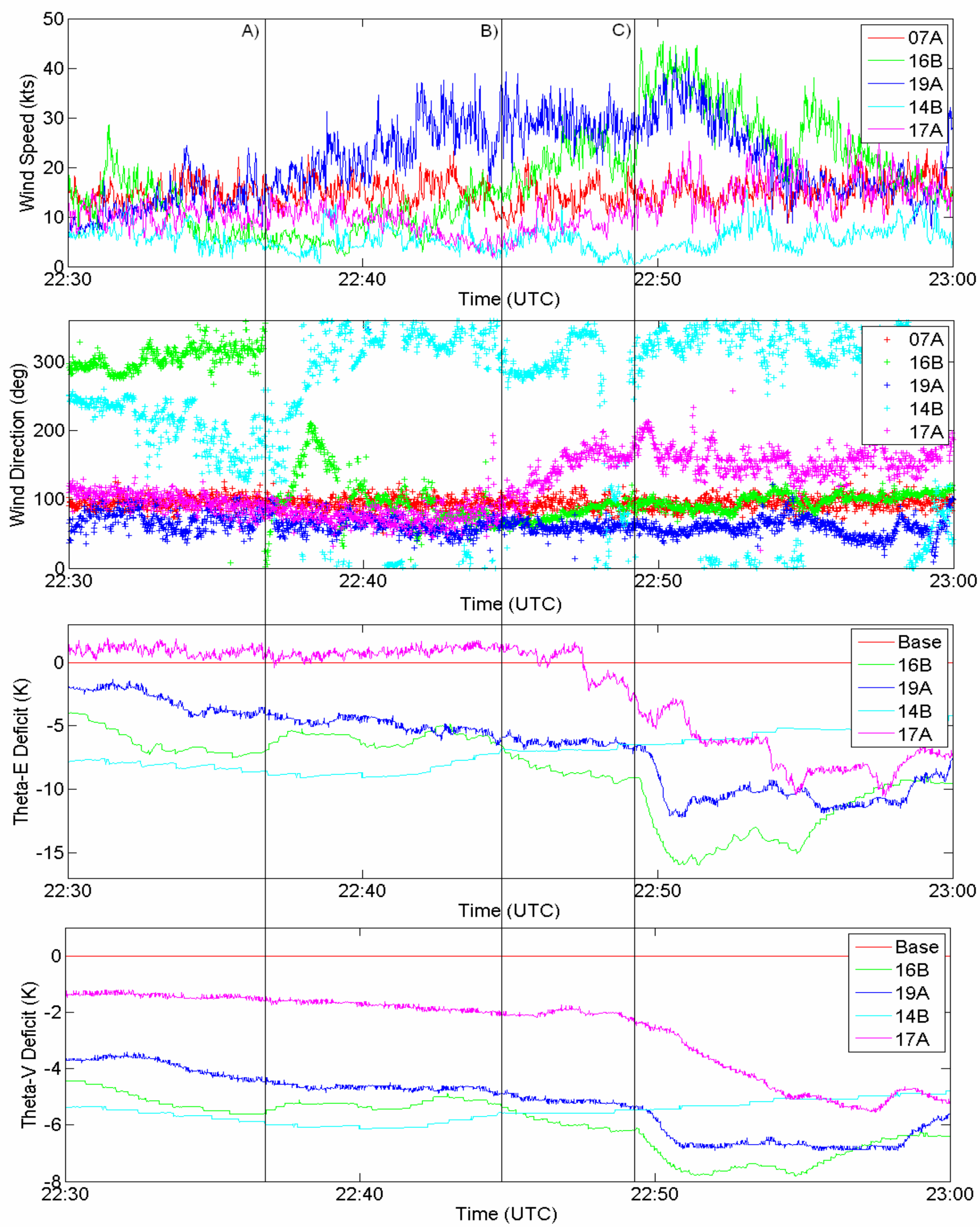

Figure 2: Time-series analysis of wind speed, wind direction, equivalent potential temperature deficit and virtual potential temperature deficit for probes 214B, 216B, 217A, and 219A. Probe 107A wind speed and direction is included as a representation of storm inflow. Fine lines A, B, and C represent the passage of the pre-existing boundary past probe 216B, passage of RFGF past probe 217A, and passage of secondary thermodynamic boundary past probes 216B and 219A, respectively.

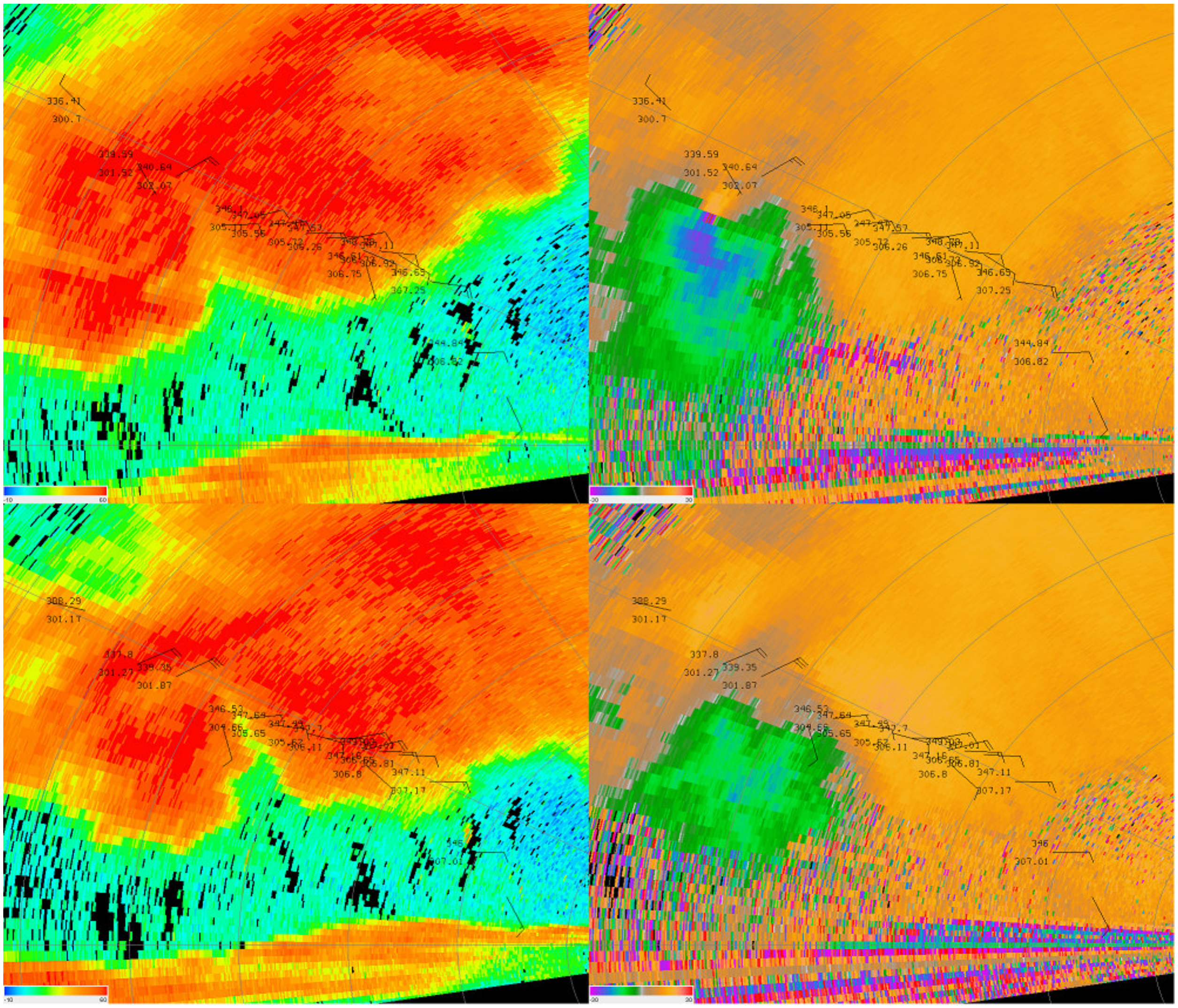

Figure 3: StickNet observations overlaid on SMART-R reflectivity (left) and radial velocity (right) scans for A) 22:39:00 UTC and B) 22:45:10 UTC. Observation plots contain equivalent potential temperature (upper-left) and virtual potential temperature (lower-left), wind observations given in kts.

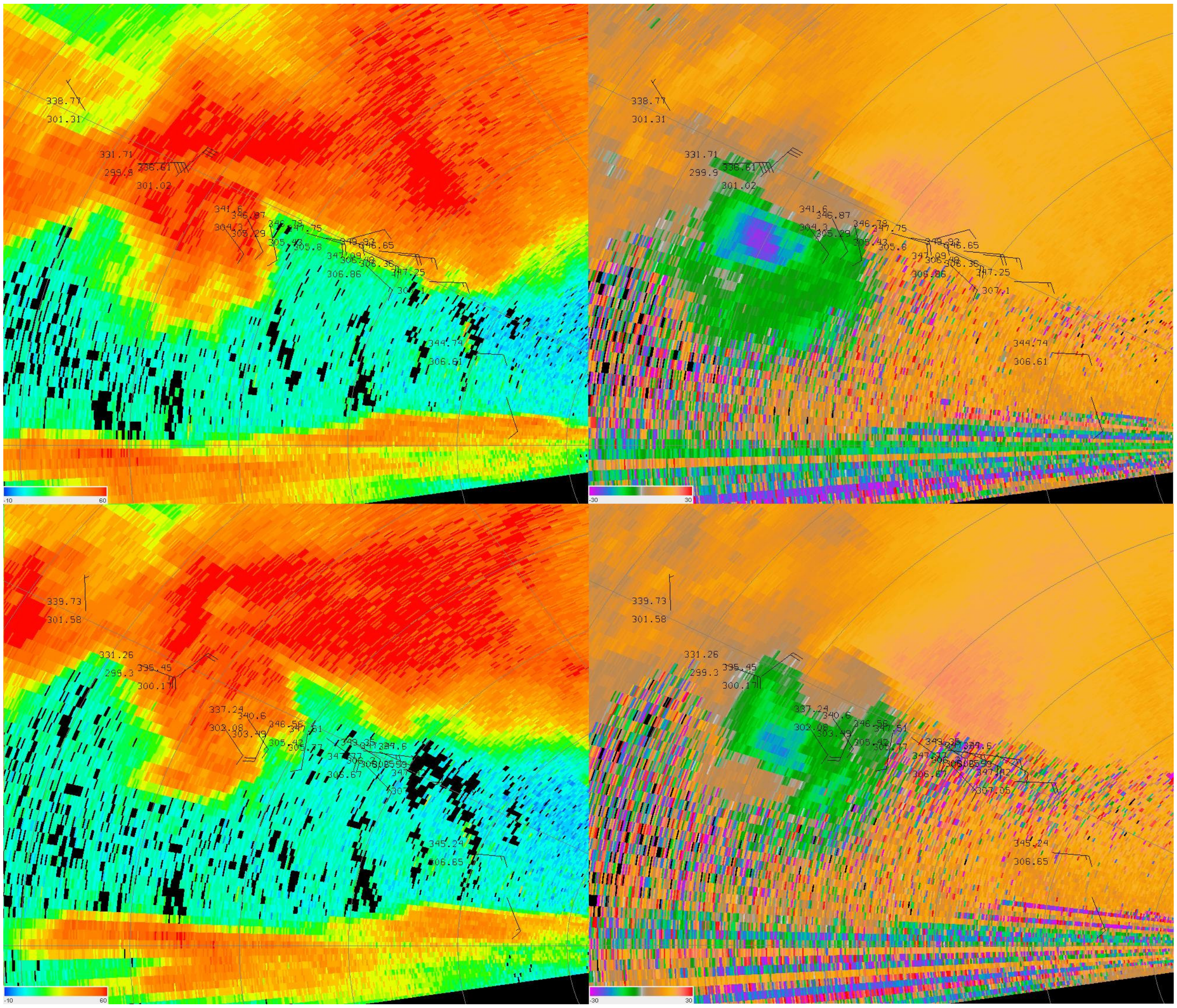

Figure 4: Same as 3, except for A) 22:50:00 UTC and B) 22:54:01 UTC.

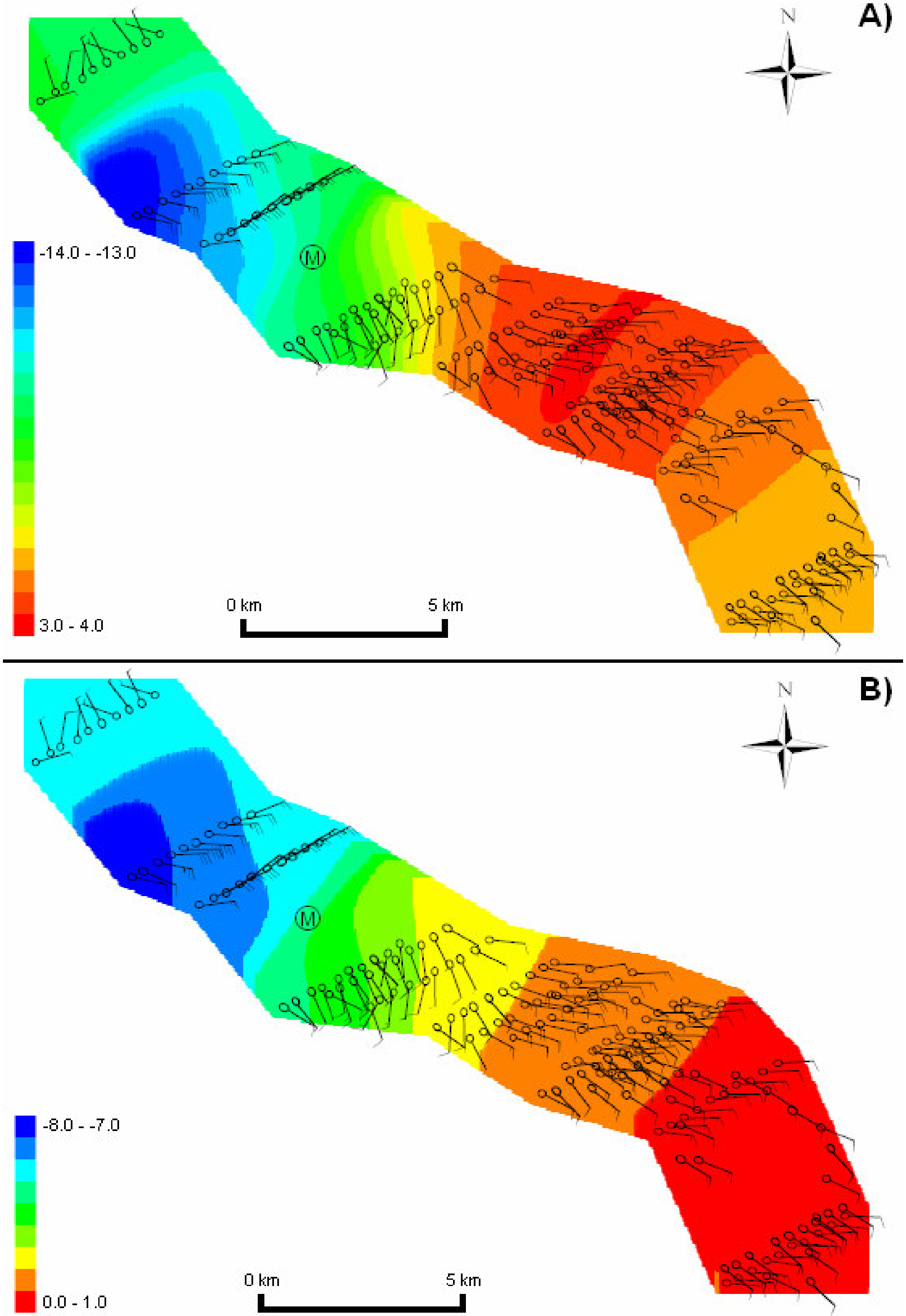

Figure 5: Time-to-space converted wind observations (kts) overlaid on objectively analyzed data for A) Equivalent potential temperature deficit (K) and B) Virtual potential temperature deficit (K) for 22:45 UTC to 22:55 UTC. "M" denotes the position of the mesocyclone on SMART-R imagery at 22:50 UTC.